Available online at www.sciencedirect.com

ScienceDirect

Advances in Space Research 75 (2025) 233–247

ADVANCES IN SPACE RESEARCH (a COSPAR publication)

www.elsevier.com/locate/asr

Estimation of land surface temperature and LULC changes impact on groundwater resources in the semi-arid region of Madhya Pradesh, India

Kanak N. Moharir [a,*], Chaitanya Baliram Pande [b,c,*], Vinay Kumar Gautam [d], Sonam Sandeep Dash [e], Arun Pratap Mishra [f,k], Krishna Kumar Yadav [g], Hany W. Darwish [h], Malay Pramanik [i], Mohamed Elsahabi [j]

[a] Department of Remote Sensing, Banasthali Vidyapith, Rajasthan
[b] Institute of Energy Infrastructure, Universiti Tenaga Nasional, Kajang 43000, Malaysia
[c] New Era and Development in Civil Engineering Research Group, Scientific Research Centre, Al-Ayen University, Thi-Qar, Nasiriyah 64001, Iraq
[d] School of Natural Resource Management, College of Post Graduate Studies in Agricultural Sciences, Central Agricultural University (Imphal), Umiam-793103, Meghalaya
[e] School of Civil Engineering, University College Dublin, Ireland
[f] Department of Forestry and Remote Sensing, Earthtree Enviro Private Limited, Shillong, 793012, Meghalaya, India
[g] Department of Environmental Science, Parul Institute of Applied Sciences, Parul University, Vadodara, Gujarat 391760, India
[h] Department of Pharmaceutical Chemistry, College of Pharmacy, King Saud University, Riyadh 11451, Saudi Arabia
[i] Urban Innovation and Sustainability Program, Department of Development and Sustainability, Asian Institute of Technology (AIT), PO. Box 4, Klong Luang, Pathumthani 12120, Thailand
[j] Faculty of Engineering, Aswan University, Aswan 81542, Egypt
[k] Earthtree Data Services Private Limited, 110024, Delhi, India

Received 6 May 2024; received in revised form 3 September 2024; accepted 12 September 2024
Available online 16 September 2024

Abstract

The land surface temperature (LST) changes influence on many factors such as land use and land cover (LULC), vegetation and water resources etc. Now a day's urban population growth, industrial development and human activity are increased due to human migration and urban expansion. The surface temperature is very harmful to vegetation, groundwater level, and ecosystem health. Urban pollution growth and air pollution factor is also playing important role for increase and decrease the LST with climate change impact. Demand of drinking water are increases particular in the urban city due to the population growth and urban expansion, which all of this direct effect on surface and groundwater sources and resources. Hence we have been chosen the latest technologies such as remote sensing (RS), Geographic information System (GIS) and Google Earth Engine (GEE) are very effective for mapping, monitoring and assessment of spatial maps of LST, LULC, and NDVI (Normalised differential vegetation index) estimation. In this study, main focus on the LULC of 2011 and 2021 were classified using random forest (RF) algorithm, ML and remote sensing datasets. LULC were divided into four categories i. e. agricultural land, built up land, waterbody and waste land. For better understanding about the growth of LST, this study examines the association between LST and NDVI change, what vegetation condition impact on the LST. The main and important results have been found the built-up land and LST positive correlation due to increases both the factors in the urban area. LST increases gradually and its bad effect on the green land, water level and expansion of barren land. The range of LST is 43.60 °C to 45.30 °C. Less vegetation cover showing highest LST and vice versa. All of the LST, NDVI, and LULC direct effect on the groundwater availability in the area. This

* Corresponding authors.
E-mail addresses: kanak.moharir1@gmail.com (K.N. Moharir), chaitanay45@gmail.com (C. Baliram Pande).

https://doi.org/10.1016/j.asr.2024.09.025

paper important result found the built-up land and LST both are increased in 2021, NDVI and LST having negative correlation. The results of study can very much useful for understanding the LST, NDVI and LULC, these factors what impact on groundwater availability in the study area.

Keywords: LST; NDVI; Climate Change; Groundwater availability; ML

1. Introduction

For the ecosystem contain the various natural resources combination of Land, water, and vegetation to balance the ecosystem system for urban cities. Land and water are expected resources that play critical roles in entire stages of living- organism life (Gautam et al., 2020; Yin et al. 2022). However, the role of vegetation in the ecosystem is critical for sustaining environmental constancy in response to climate change (Guo et al., 2014; Wang et al., 2018; Gautam et al., 2023). LULC means the changes in land cover, i.e., the biophysical attributes of the land terrain, and land use is utilization of the Land for human purposes. It provided information on the primary determination of environmental changes (Zhou et al. 2023a, 2023b; He et al. 2024). The research absorbed on LULC change offers valuable insights into comprehending past practices, and the anticipated trajectory of future LULC patterns (J. Kabeto et al., 2022, Hussain, S.et al., 2020 a and b). Peng et al., (2019); Song et al., (2018); Kamyar Fuladlu (2022) utilized diverse vegetation's indices and LULC maps derived from different bands of satellite imagery to assess the fluctuating patterns of LST across various physical and cultural landscapes. Khan et al. (2020) understands the change detection method, which has classified into three components, i.e., pixel level, features level, and object level image processing (Akhtar et al., 2020; Abdullah et al., 2019; Hussain et al., 2020; Ali et al. (2018)). Vohra and Tiwari (2023) found the LST higher degree in the built-up classes due to LULC changes and the alteration of built-up parts. The simulation outcomes shown the built-up part rises up to 81 %, and greenness area declined by − 65 % in the year of 1994–2018. This study more important analysis of LULC maps impact on the LST and groundwater resources changes in the area. Compared with other the studies, our work is more important for the understanding the relations LST and groundwater resources due to LULC, NDVI and water levels. Other studies only shown the relation s]of NDVI and LST correlation analysis but this paper work so much LST impact on the groundwater resources.

The NDVI delivers a precise representation of the plant cover by applying analysis based on satellite datsets (Roy et al., 2021; Zhao et al. 2024a; Li et al. 2023). Scientific studies shown that healthy vegetation are extremely reflective of near-infrared (NIR) light (0.7–1.1 m) and highly absorbent of visible light (0.4–0.7 m). NDVI values differences are typically between −1 and 1 range indicated the vegetation health or not health on the earth surface (Rambe, 2020; Liu et al. 2024; Xie et al. 2023). Babalola & Akinsanola, (2020) observed that values larger than 0.2 shows the vegetative cover and a highest range represents the dense greenness cover. The NDVI is a valuable index for analysing the green body performance at the landscape pattern, while the productivity of vegetative covers is related to evapotranspiration and rainfall (Hussain et al., 2022; Li et al. 2024; Zhao et al. 2024b). The NDVI values were interrelated with the plant's biological events, and variation of NDVI indicates the various ecological tasks in vegetation (Abou Samra and El-Barbary (2018); Yin et al. 2023a; 2023b). The daily fluctuations in LST may be clearly defined using NDVI value, which shows the vegetation canopy (Kharazmi et al., 2018; Hussain & Karuppannan et al. 2023; Abou Samra (2022)). In recent years, research investigations have trusted extensively on remote sensing and GIS data to map specific vegetation kinds and explain the diversity of vegetation (Pal & Ziaul, 2017; Romaguera et al., 2018; Zhou et al. 2023c). The geospatial technique is an essential tool for monitoring the urban settlement, land use mapping, vegetation extents of NDVI, and environmental implications of urban growth during specific periods (Bansod & Dandekar, 2018; Khan et al., 2020; Hussain et al., 2022).

The relationship among the LST and LULC have been investigated the ecological effects of LST further and report local environmental issues (Abera et al., 2019; Hussain, S., et al. 2023; Zhang et al.2022). The LST represents the soil surface temperature in the upper section direct effect on the vegetation and ecological system (Begum et al., 2021; Zhao et al. 2023; Yi et al. 2022). The density of vegetation correlates with reduced temperature variability, which means that as vegetation density grows, so does the range of temperature fluctuations (Tafesse & Suryabhagavan, 2019). Furthermore, the increase vegetation during warm days might contribute to a decrease in LST, which helps to control the sense of temperature (Kimuku & Ngigi, 2017; Mukherjee & Singh, 2020; Salahi & Behrouzi, 2023; Hussain, S. et al. 2022).

The LST trends given the valid environmental data that assists the understanding of the climate variability (Athick et al., 2019; Yamamoto & Ishikawa, 2020; Abou Samra (2023)). These are influenced by numerous elements, including soil composition, vegetation changes, building materials have been used on the roads, and impermeable

and susceptible surfaces (Cai et al., 2018; Sadiq Khan et al., 2020). Guha and Govil (2023) have been relationship with correlation between LST and four indices such as Modified Normalized Difference Water Index (MNDWI), and NDVI for India region by using Landsat-8 data. The association between the LST and LULC parameters could be observed differently for every season. The LST values represent how the land surfaces change in the seasons. The Landsat satellite series offers high-resolution LST estimates, which are especially useful for study on a smaller scale or in an additional localized area (Sajan et al., 2023; Waleed, M., et al; 2022; Zhao et al. 2024). In winter, the weather is mostly dry due to low humidity, which also means there is a little greenery. As a result, the correlation between the LST and LULC indices should be different in winter than in other seasons. Therefore, the current study has used four Landsat 7 and 8 data (April 2011 to April 2021) for the Panna district to assess the uniform properties of the LULC indices. Also, whole past research works examination one or more LULC keys. Thus, the main objective of this paper is to study the spatial–temporal variation pattern of the LULC, LST, and NDVI in the Panna District of Madhya Pradesh state and its will create the relationship of LST with NDVI for understanding the LST changes and impact on groundwater availability with LULC changes with LST effect on the groundwater availability in the central India.

2. Materials and methods

2.1. Study area

It is situated in the north-eastern side of Madhya Pradesh State. This area is famous for diamond mines, located 80 km around Panna town. The population of the district is nearly 10, 16,520; the district lies between 23.45°N 79.45°E and 25.10°N 80.40°E. The total area of 7135 km^2 is covered. Continuing Meadows is interspersed with forests, hills, and evergreen trees in the Panna district. The Panna district comes under the Bundelkhand region, which is a drought-prone area in the country. However, drought frequency and intensity have been increased in recent decades. The 41 % rain deficit rainfall this is critical zone of drought-prone area. The Panna tiger reserve overlays a wide-ranging dense forest with a promising diamond quarry. Active mines exist both to the east and west of the corridor. This area has been transformed into a natural woodland and flora city with a sanctuary for unique wildlife, and avifauna and a diamond mine. The location of study area is presented in Fig. 1.

2.2. Rainfall and climate

Panna district receives a moderate to high annual average rainfall, contributing significantly to the groundwater recharge. The district experiences a monsoon-dominated climate, with the southwest monsoon bringing rainfall between June and September (Gautam et al., 2021). The rainfall infiltrates the ground, replenishing the aquifers and maintaining the groundwater levels. The average annual rainfall is 1066 mm (CGWB, 2013). With scorching summers, a relatively more relaxed monsoon season, and chilly winters, Panna has a humid subtropical climate.

2.3. Soil type

Around 75 % of the district's total area is characterized by alluvium soils resulting from Vindhyan sediment weathering. In the northern section of the district, yellowish sandy soils prevail, originating from the weathering of granitic rocks. Moreover, the river courses within the district contain extensive deposits of thick alluvial soils (CGWB, 2013). The district area has rich geology (alluvial plain) and is flat near the Ken River, which is ideal for agricultural activities.

2.4. Geomorphology

The Bundelkhand upland has an average elevation of 170 mean sea levels (MSL). The gently sloping surface eroded over time, featuring mesa and linear ridges dispersed throughout the area. The study area is underlain by the Vindhyan supergroup, Limestone and Sandstone and Alluvium (CGWB, 2013). The Vindhyan supergroup consists of Bhander Shale, Sandstone, and Limestone. The abundance of columnar stromatolites characterizes the Bhander limestone, while the limestone lacks them (Gautam et al., 2023).

3. Geology and hydrogeology

The Panna district is in the northern part of the Vindhyan ranges and is characterized by a diverse geological environment. The region consists of sedimentary rocks with significant aquifer potential, including sandstones, shale, and limestone. Fractured and weathered zones in the rock formations enhance the groundwater refresh and storage capacity (Gautam et al., 2021; Gautam et al., 2022). Alluvium soils formed by the weathering of Vindhyan sediments cover nearly three-fourths of the territory. The river courses are covered in thick alluvial soils (CGWB, 2013). Localized patches of alluvium cover are found along the banks of the district's major and minor rivers and streams. The thickness of alluvium is greater in granitic rocks and shales and less in sandstone and limestone formations. (Trivedi et al., 2022; Gautam al., 2023). CGWB has installed 20 Groundwater Monitoring Wells and 4 Piezometers in the district to monitor seasonal and annual groundwater quantity and quality fluctuations. Analyses of pre-monsoon groundwater level data indicate a concerning downward trend in water level in the entire district, with a few exceptions (Moharir et al., 2023).

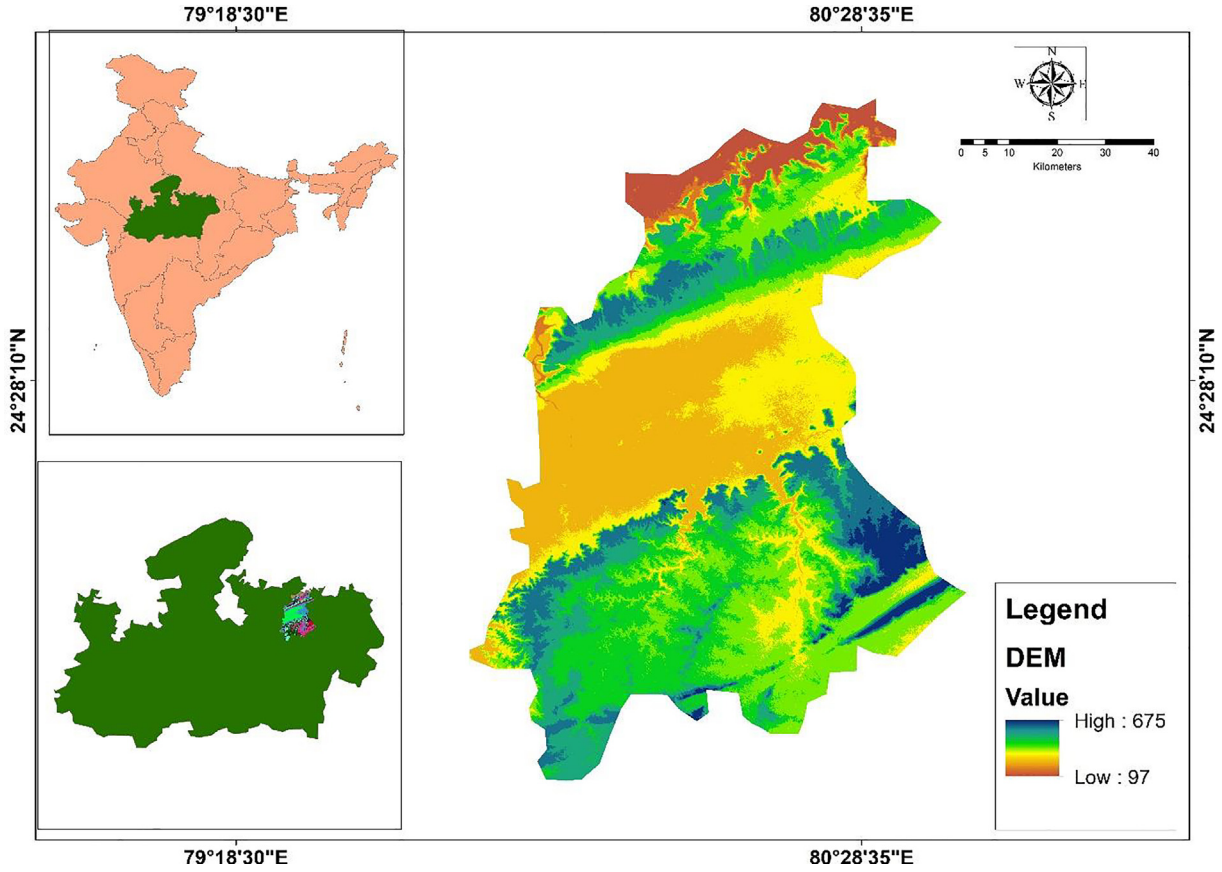

Fig. 1. Location map of study area.

4. Data

The present study investigates the correlation between LST and NDVI in the drought-prone city of Panna in the Bundelkhand region. This study focuses on 2011 to 2021 to analyse the fluctuations in green cover and LST. Specifically, the summer season has been chosen for examination because satellite data was very clear for vegetation visibility during this time. Landsat-8 and 7 are images from the US Geological Survey website (Table 1). Landsat seven and eight images from 2011 and 2021 have been used to compute the LST and NDVI.

4.1. Methodology

The GEE platform is a very powerful cloud platform for data access and processing, with the development of algorithms for creating spatial maps and scientific analysis. In this study, we prepared various thematic maps such as LULC, NDVI and LST based on the Landsat 7 and 8 satellite data from April 2011 to April 2021. The satellite data and other information are presented in Table 1. The satellite datasets were atmospheric and geometric corrected before the classification of maps. The NDVI and LST index were estimated based on the GEE algorithms and remote sensing datasets (Pande et al. 2024). The GEE platform for this study analysis accesses all of the datasets.

LULC mapping and change detection maps were prepared with the help of GEE and ML models. The RG model was used in this study to prepare LULC mapping using the GEE platform. This methodology developed the novel methods and effectively classified the LULC classes maps and change detection, and this GEE platform totally cloud with developed algorithms using JAVA script (Pande, 2022). LULC maps validated with ground truth datasets in the classification of satellite images. In this research, we have created an RF model generally related to the ML approach to find the LULC classes in the area. The years of NDVI, LST and LULC maps have been used to determine groundwater availability in the study area.

Table 1
Details of satellite data and resolutions.

Satellite data	Sensor	Date of acquisition	Path and row	Number of Bands	Spatial resolution (m)	Sources
Landsat 7	ETM +	2011/04/20	187/52	07	30 and 60	https://earthengine.google.com/
Landsat 8	OLI_TIRS	2021/04/20	187/52	08	30 and 100	

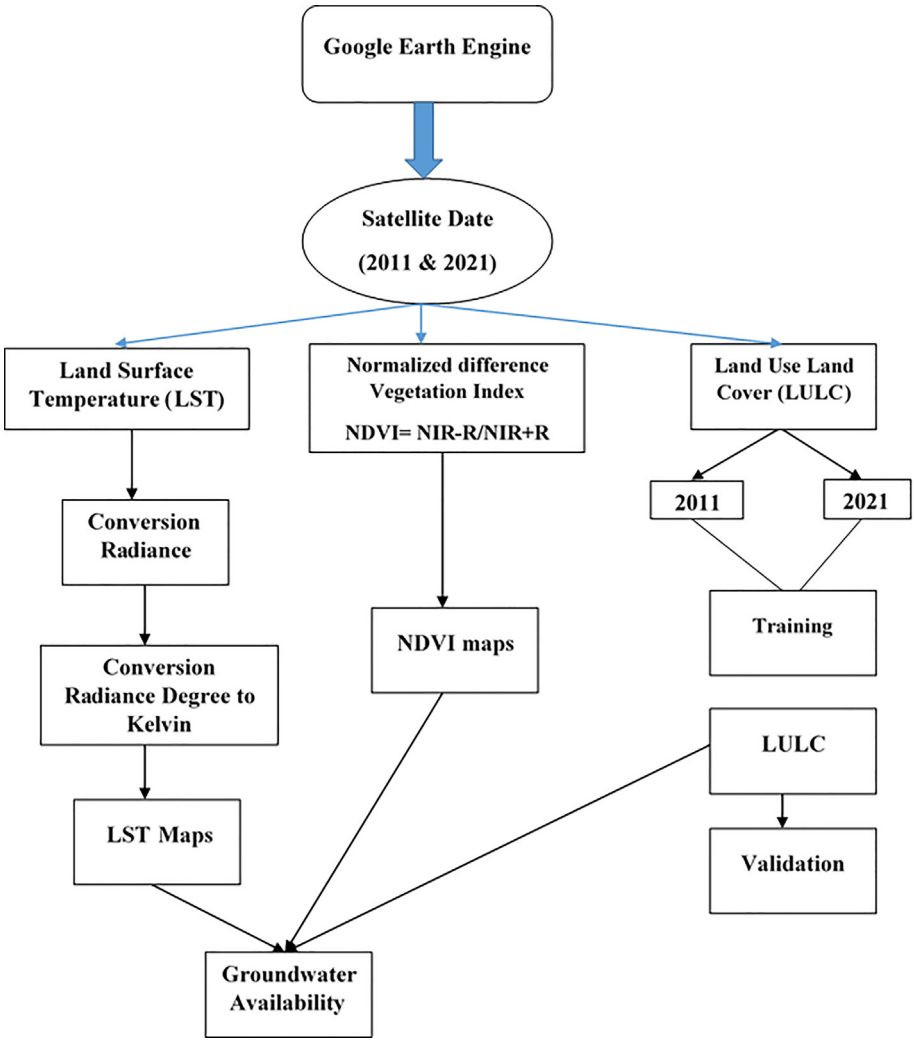

Fig. 2. Flow chart of methodology.

The climate datasets were used for the validation process and assessment. The methodology of the flow chart is shown in Fig. 2.

5. Satellite imagery pre-processing

The satellite data acquired from the GEE platform is calculated for LST, NDVI, and LULC change detection; these factors impact groundwater conditions. The Landsat 7 ETM + and Landsat 8 OLI_TIRS path and row are 187/52 in Landsat 7, numbers of bands seven and 8, 11 bands are presented. The reflected and emitted energy from the earth's surface is assembled and measured by an imaging radiometer, ranging from visible to thermal infrared. Detailed information on satellite datasets is presented in Table 1.

6. LULC mapping

It played a vital role in this study because the Panna district is a drought-prone area, and water scarcity is a huge issue. Hence, within ten years, there is a drastic change in built-up land. The RF model has been used in LULC classification. Compared to a single classifier, Classifier ensembles work by performing classifications through a series of joint classifiers. The Random Forest method, proposed by Breiman (2001), encompasses several benefits for remote sensing applications. The forest is an arrangement of the formation of decision trees, and its signification is very difficult in the random forest method. Hence, two steps are used for identification. In the first step, individual trees are created by randomly selecting the samples, wherein each selected tree is trained to assign unique samples of uniform sizes. In the second step, each tree node determines the constraints by comparing predictor variables. The random forest method usually employs the Gini index. It is denoted in Eq. (1):

$$\sum\sum_{i+j}(f(C_i,\ T)/\mid T\mid),(f(C_j,\ T)/\mid T\mid) \tag{1}$$

where $f(C_i,\ T)/|T|$ is the possibility of given case belonging to C_i class. Hence, a decision tree is form with the help of particular characteristics combination extends it is to full depth without pruning.

6.1. Accuracy assessment

It is a crucial stage in evaluating various image processing techniques, particularly in classification tasks. The error matrix serves as the primary method for presenting accuracy assessment, providing a comprehensive overview of classification performance. Producer accuracy, user accuracy, and overall accuracy are key metrics calculated using Eq. (2) (Hussain et al., 2022).

$$\text{Overall accuracy (Oc)} = \frac{\textit{Number of sampling classes classified correctly}}{\textit{Number of reference sampling classes}} * 100 \quad (2)$$

The kappa (K) values measure how well RS classification agrees or is accurate with the reference data. A statistical representation of kappa (K) is as in Equation (3) (Safder, 2019) (Table 2 and 3).

$$K = \frac{\textit{Observed Accuracy} - \textit{Chance Assessment}}{1 - \textit{Chance Agreement}} \quad (3)$$

7. Results and discussion

This study focuses more on the GEE and RS technology. The advancement of Earth observation satellites have resulted in abundant, an easily accessible data from various open access platforms. The GEE has emerged as a widely utilized tool in recent years due to its cloud-based geospatial analysis and modelling capabilities, freely and readily available to researchers for scientific analysis. With GEE platform can view, observe, and interpret geospatial data for many applications applied by researchers. Moreover, integrating ML algorithms with GEE has further enhanced the accessibility and analysis of geospatial data. This combination proves that is beneficial for generating multi-temporal images and providing practical environmental monitoring tools. The LULC is divided into five classes then. This class changed the direct impact on the LST and groundwater resources NDVI values in 2011 and 2021, offering insights into vegetation health over the specified timeframe. The seamless integration of remote sensing technologies, GEE, and ML algorithms has empowered researchers to obtain comprehensive data for studying environmental changes and land cover transformations, fostering more informed decision-making processes and contributing to various environmental monitoring applications. This amalgamation of advanced technologies is significant for understanding Earth landscape's dynamic nature. It contributes significantly to the scientific community's ability to monitor and assess environmental changes effectively. Hence this technologies more effective to monitoring, development spatial maps for better understanding the LST, NDVI, LULC changed and relationship with groundwater resources and availability.

Table 2
Accuracy Assessment of 2011.

	Built up land	Waterbody	Agriculture land	Waste land	Total (Users)
Built up land	9	0	0	0	9
Waterbody	0	9	0	0	9
Agriculture land	0	0	10	2	12
Waste land	0	0	0	10	10
Total Accuracy	9	9	10	12	40

Table 3
Accuracy Assessment for 2021.

	Built up land	Waterbody	Agriculture land	Waste land	Total (Users)
Built up land	9	0	0	0	9
Waterbody	0	8	2	0	10
Agriculture land	0	0	9	2	11
Waste land	0	0	0	10	10
Total Accuracy	9	8	11	12	40

8. Estimation of NDVI

The GEE has a function for calculating NDVI from an image using the red and NIR frequency bands. Separate NDVI functions were used since Landsat 5 and 8 have various band combinations for obtaining their NIR band spectra. Landsat 5 uses band 3 for the red and 4 for the NIR bands, whereas Landsat 8 uses band 4 for the red band and band 5 for the NIR band. The NDVI is the most common and widely used index for identifying the present growth of vegetation in this study. Generally, the positive value of NDVI indicates green vegetation. NDVI > 0.5 shows dense coverage of green and healthy vegetation. In this study, we have calculated the NDVI values using algorithms to connect with the effect of LST on vegetation. The higher value of NDVI signifies the integrity of vegetation cover, while the lower values denote the opposite trend. The NDVI was estimated from Landsat images and had characteristic values between -1 and 1. NDVI was calculated by the following formula Eq. (4):

$$NDVI = \frac{NIR - R}{NIR + R} \quad (4)$$

Where, NIR is near-infrared band (TM and ETM band 4, OLI band 5) as well as R is the red band (TM and ETM band 3, OLI band 4). The following Fig. 3 a and b shows the NDVI maps of 2011 and 2021.

9. LST estimation

Many types of research related to hydrological processes increasingly depend on LST. The advancement in satellite datasets have been improved the calculation of LST through thermal radiance LST, which is a significant factor in controlling environmental, biological, chemical, and socio-economical processes on the earth (Moharir et al.,

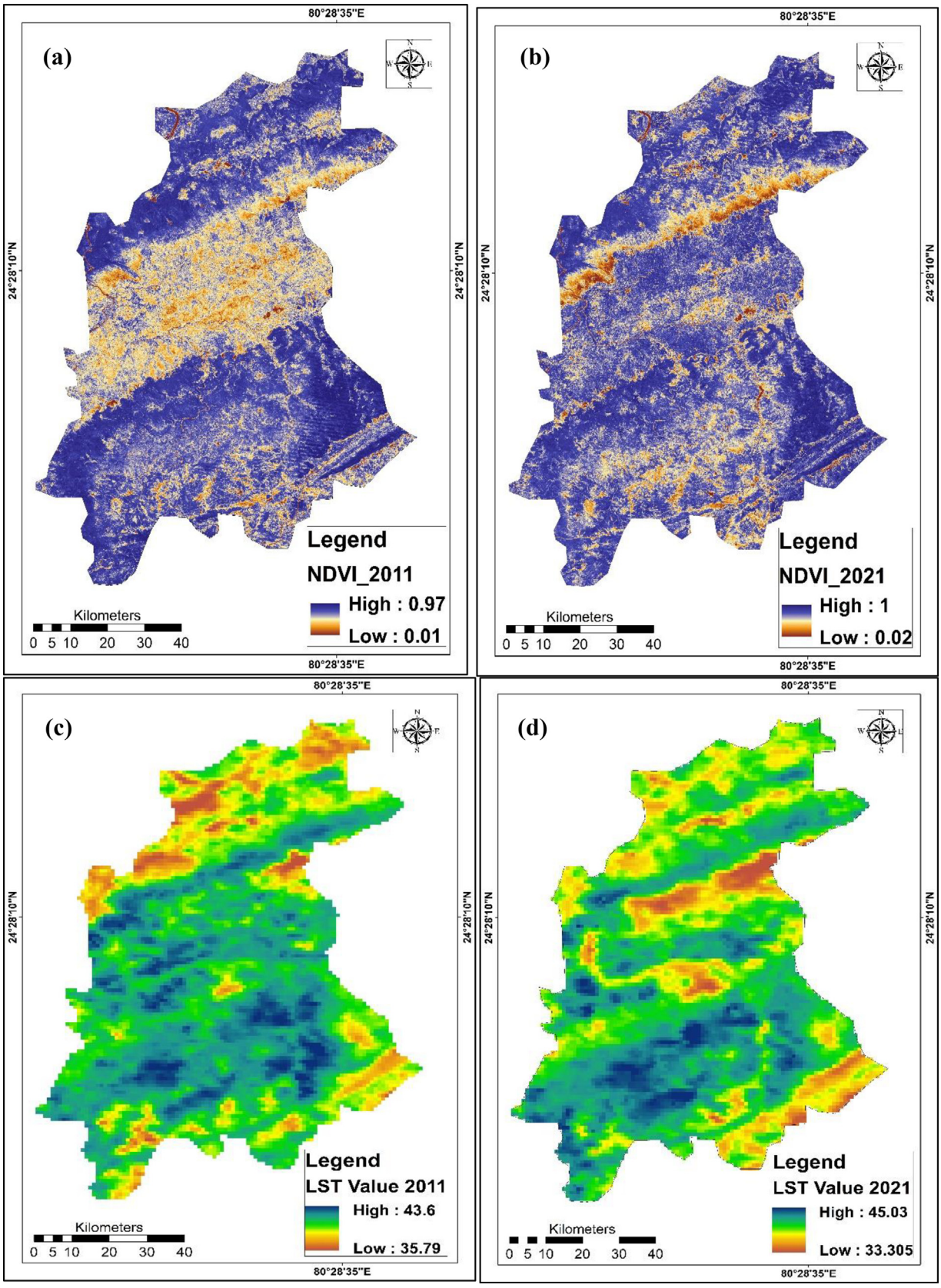

Fig. 3. (a) NDVI map 2011 of study area. (b). NDVI map 2021 of study area. (c). LST map 2011 of study area. (d) LST map 2021 of study area.

2023; Abera TA et al., 2019). The day by increased the built-up land directly contribution to LST changes and increases, which of LST values effect on the groundwater resources and urban ecosystem. It is observed that the built-up land density to direct bearing on the LST. In the study area, despite the crops, the densely built-up land area shows the highest LST. The LST is calculated using a multi-temporal Landsat-8 and Thermal Infrared Sensor (TIRS), and it was performed in Arc GIS 10.5 using the raster calculator tool (Fig. 3 c and d).

The atmospheric brightness temperature was calculated using following Eqs. (5) and (6):

$$\mathrm{Tb} = \frac{K_2}{\ln\left(\frac{K_1}{L_\lambda}+1\right)} \tag{5}$$

Where K1 and K2 values are 607.76 and 1260.56 for Landsat 4/5 (TM), and 772.88 and 1321.07 for Landsat 8 (OLI), respectively (Eq.6).

$$\mathrm{L}\lambda = gain \times QCAL + offset \tag{6}$$

Where Lλ represents spectral radiance and QCAL is quantized calibrated pixel value in DN.

After the calculation of atmospheric brightness temperature, the next step was to compute the proportion of vegetation (Pv) using NDVI index. The following formula was used to calculate the Pv in Eq. (7):

$$\mathrm{Pv} = \left(\frac{NDVI - NDVI_{min}}{NDVI_{max} - NDVI_{min}}\right)^2 \tag{7}$$

After that, land surface emissivity was computed with the following Eq. (8).

$$\varepsilon = 0.004 \times \mathrm{F}_V + 0.986 \tag{8}$$

where, ε = surface emissivity and Fv = fractional vegetation

Finally, LST is computed by Eq. (9) … (Weng et al., 2004):

$$\mathrm{LST} = \frac{T_b}{1 + (\lambda_\sigma/(h_c))\ln\varepsilon} \tag{9}$$

where, λ = effective wavelength, σ = Boltzmann constant (1.38×10^{-23} J/K), h = Plank's constant (6.626×10^{-34} Js), c = velocity of light in a vacuum; (2.998×10^{-8} m/sec), ε = emissivity.

10. LULC accuracy assessment

The accuracy examination of LULC maps and classifications is a crucial process that evaluates the result's quality and reliability. It is involves comparing the classified LULC datasets with reference data to define the accuracy of the classification results. This assessment is essential for various applications, including land management, urban planning, environmental monitoring, and natural resource assessment. The Kappa coefficient method is widely employed to evaluate the accuracy of classified data based on image analysis. The Kappa coefficient yields a value ranging from −1 to 1, where 0 indicates no difference between random and trained classifications.

A confusion matrix is utilized to quantify accuracy further, enabling the computation of overall accuracy (OA), producer accuracy (PA), and consumer accuracy (CA) (Pande, 2022). The OA is computed by using the formula i.e. total number of correct selections separated by whole number of samples multiplied by 100 %. The PA was determined as 100 % minus the omission percentage, and the CA was calculated as 100 % minus the error of commission percentage. The kappa coefficient formula incorporates diagonal frequency (a), total frequency (N), and expected frequency (ef) in its calculation. This formula is significant in assessing the contract among classified data and reference data, providing valuable insights into the accuracy of the LULC classification. The LULC maps of 2011, 2021 are presented in Fig. 4a and Fig. 4b, respectively. These maps reflect the outcomes of the accuracy assessment and highlight the spatial distribution of different LULC classes within the Panna District area over the specified periods is shown in Equation (10)….

$$KC = \frac{\sum a - \sum ef}{N - \sum ef} \tag{10}$$

Where "a" denotes diagonal frequency, "N" denotes total frequency, and "ef" denotes expected frequency.

Overall accuracy

$$= \frac{\textbf{\textit{Number of sampling classes classified correctly}}}{\textbf{\textit{Number of reference sampling classes}}} * 100$$

$$= \frac{38}{40} \times 100$$

$$= 95\%$$

$$\textbf{Kappa Coefficient}\,(\mathbf{T}) = \sum$$

$$= \frac{(\textbf{\textit{TS}} * \textbf{\textit{TCS}}) - \sum(\textbf{\textit{Column Total}} * \textbf{\textit{Row Total}})}{TS2 - \sum(Column\,total - Row\,Total)} * 100$$

$$\frac{(40*38) - \{(9*9) + (9*9) + (10*12) + (12*10)\}}{1600 - \{(9*9) + (9*9) + (10*12) + (12*10)\}} * 100$$

$$= \left(\frac{1520 - 985}{1600 - 985}\right) * 100$$

$$= 82\%$$

Here, TS = Total Sample = 40

TCS = Total correct Sample = 38

$$= \frac{36}{40} \times 100$$

$$= 90\%$$

$$\textbf{Kappa Coefficient}\,(\mathbf{T}) = \sum$$

$$= \frac{(\textbf{\textit{TS}} * \textbf{\textit{TCS}}) - \sum(\textbf{\textit{Column Total}} * \textbf{\textit{Row Total}})}{TS2 - \sum(Column\,total - Row\,Total)} * 100$$

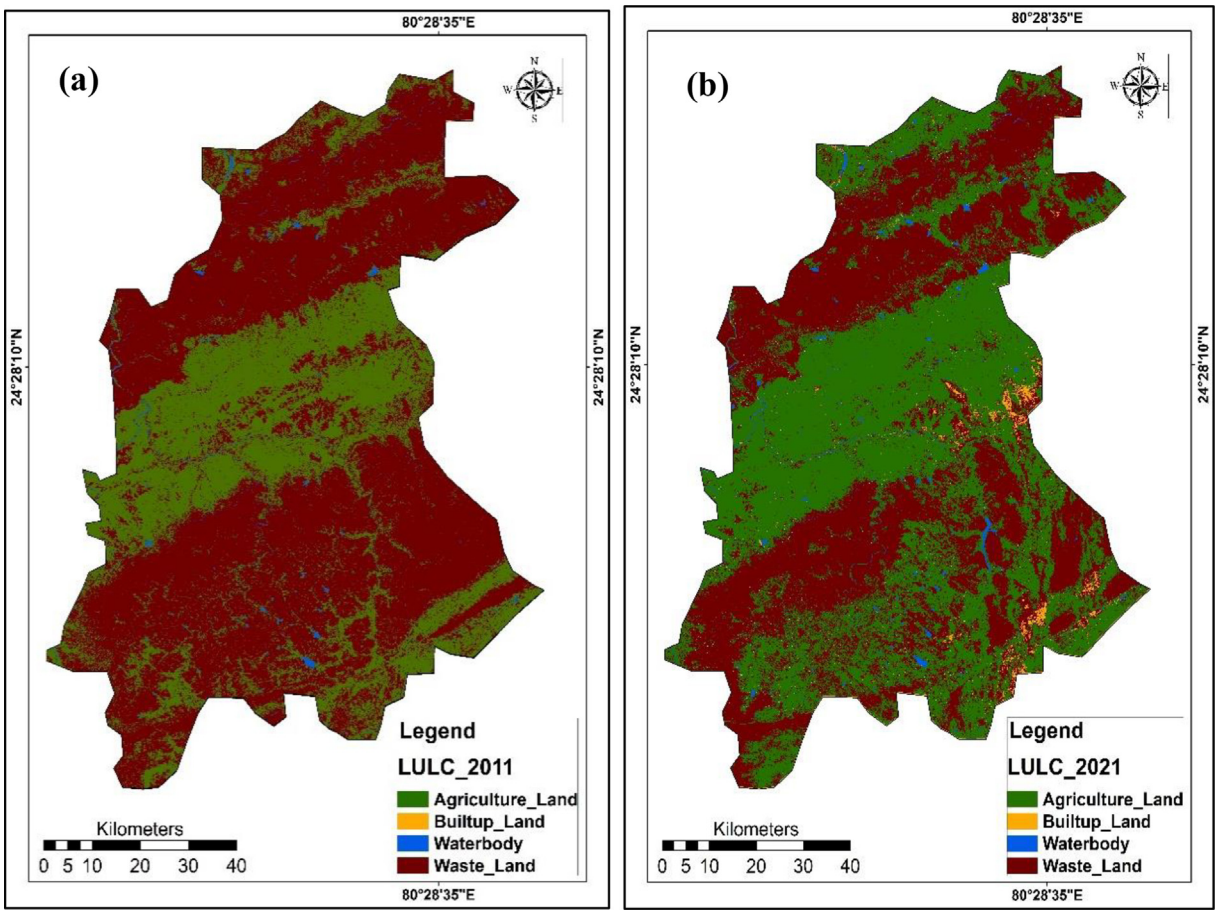

Fig. 4. (a) LULC map 2011 of study area. (b) LULC map 2021 of study area.

$$\frac{(40*36)-\{(9*9)+(8*8)+(9*11)+(12*10)\}}{1600-\{(9*9)+(8*8)+(9*11)+(12*10)\}} *100\cdots$$

$$=\left(\frac{1440-985}{1600-985}\right)*100$$

$$=80\%$$

Here, TS = Total Sample = 40

TCS = Total correct Sample = 36.

11. Classification accuracy assessment

Based on GCP i.e. ground control points, google earth pro, latitude (X), and longitude (Y), the accuracy assessment of classified imageries utilized in the estimation of accuracy of spatial maps. There are 40 GCP selected for 2011 and 2021, compared with downloaded satellite images for 2011 and 2021. It is concluded that the total accuracy of classified images was 95 % and 90 % in 2011 and 2021, respectively. Furthermore, the Kappa Coefficient (T) of 2011 is 82 % and in 2021 80 % respectively.

a. *Change detection*

The rapid growth of anthropogenic activity and its impact on LULC changes over ten years from 2011 to 2021. All of this change undoubtedly directly impacts groundwater resources and availability. With the world observing a significant increase in human activities and urbanization, monitoring and understanding LULC changes has become crucial for environmental management and sustainable groundwater development. GEE was employed for LULC classification due to its well-established accuracy and reduced human error. These study findings showed the variations in various LULC classes for 2011 and 2021. The agricultural land experienced a slight drop, with its entire extent reducing from 993,902.06 and 969,096.2 Ha. in 2011 and 2021, respectively. The decline in cropland specifies the potential tasks in food safety and agricultural productivity in the area. In plain contrast, the class of built-up land has shown an amazing growth rate of 79.35 %, increasing from 10,724.21 and 19,233.84 Ha. in 2011 and 2021, respectively. This important rise in the urban areas shows quick growth and the growth of human settlements and structures. Such urban sprawl can have far-reaching suggestions on usual ecosystems, biodiversity, and quality of lifecycle for the residents. The wasteland category, representing perchance degraded land, saw an uncertain increase of 2.97 %, with its coverage rising from 597,644.65 to 612,798.4 Ha. In 2011 and 2021, respectively. Although the rise was not as affected as built-up land, it highlights the essentials for

natural land recovery and helps plans to address land degradation and its related ecological significance. Their area increased by 25.11 %, rising from 17,230.02 to 18,372.67 Ha. in 2011 and 2021, respectively.

To further understand the relative amounts of every LULC class, the investigators obtained the percentage area of every class in 2011 and 2021, respectively. In 2011, agricultural land controlled the landscape, occupying 83.45 % of the whole area, while built-up land accounted for 4.15 %, wasteland for 6.83 %, and water bodies for 5.57 %. However, in 2021, there was an important change in land use patterns. The quantity of agricultural land was reduced to 59.84 %, representing failure in farming activities and possible land use change. Meanwhile, built-up land remarkably raised to 1.19 %, reproducing the ever-expanding built-up parts. Wasteland classes are the main LULC classes with 37.84 % coverage, representative and rising concern for land degradation and possible desertion. Water bodies remained quite stable at 1.13 % of the area, highlighting the importance of protection efforts to protect these important resources.

These results shed light on the active and disturbing changes of LULC and LST maps, presented in Fig. 5A to C. The large growth in urbanized areas, the decline in agricultural land, the increase in wasteland, and changes in water body amounts are important for groundwater availability and ecological challenges. These tasks have a healthy impact on the LST. When the NDVI value enlarged concurrently, the LST value declined because land temperature and vegetation cover were powerfully interweaved. In contrast, a temperature rise can cause an important decline in the population of numerous tree species due to their low tolerance to high levels of temperature and CO2. With correlation coefficient −0.8293656 (t = -7.8549, df = 28, p-value < 0.001). The results underscore the significance of the impact on the LULC policy, conservation plans, and sustainable growth observed to mitigate opposing ecological influences and guarantee a more stable and strong urban landscape (see Fig. 6).

12. Influence of land use and LST impact on groundwater availability mapping

The LULC maps and change detection in the Panna district play an important role in affecting groundwater availability. The district shows various landscapes, including agricultural lands, forests, and built-up land, impacting the groundwater potential. Agricultural activities, particularly irrigation, contribute to groundwater recharge, affecting groundwater availability. This study used ten years of data to develop the relationship between LULC variations and groundwater availability. It is detected that throughout the period, there was a rise in the built-up land, which directly correlated with the correlated the increased LST in particular areas. The increased LST can harmfully affect groundwater availability due to enlarged urbanization and heat island effects with the demand for freshwater resources. This research discovered a trend in agricultural land, which will be reduced by 2.50 % in 2021. This decrease could affect groundwater availability and agricultural efficiency in the area.

GEE, Arc GIS 10.5 software and ML algorithms was applied to estimation of groundwater availability in the study area. The software simplified a complete analysis of

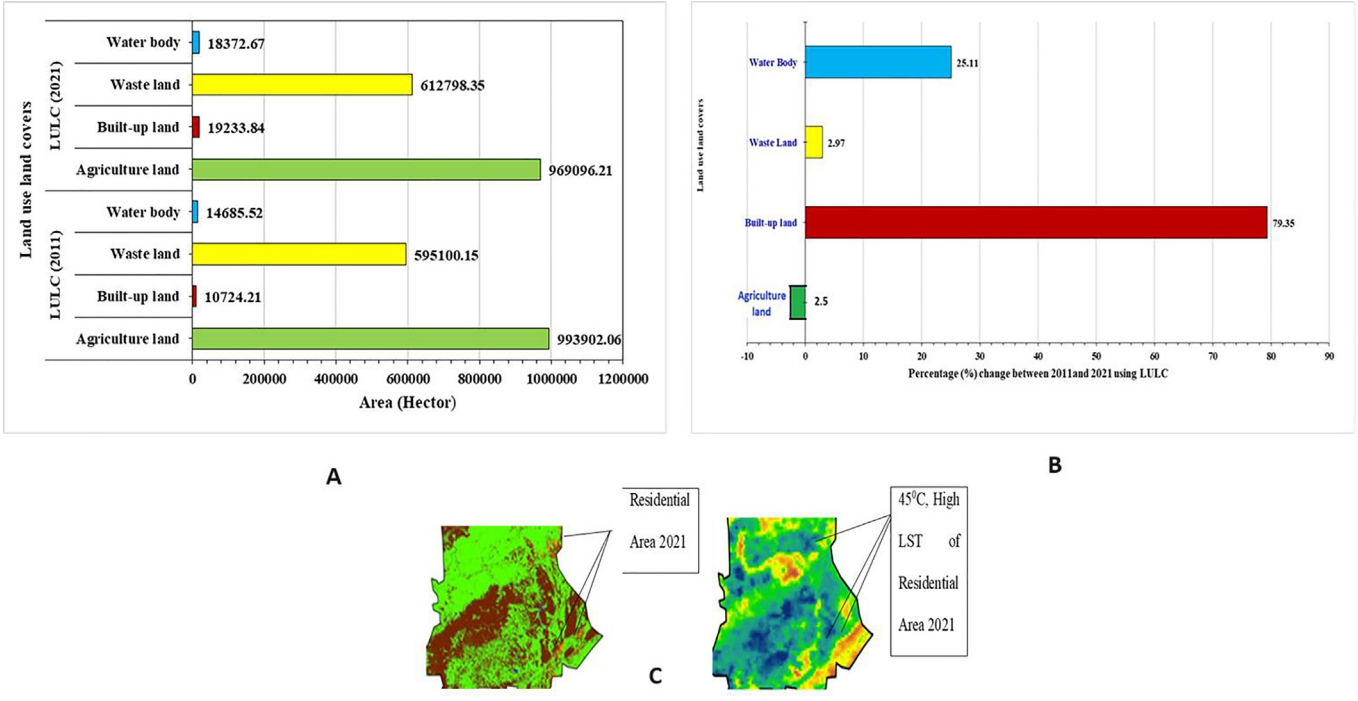

Fig. 5. A)The area of different land use categories, B) LULC changes(%) between 2011 and 2021, C) showing the residential area and its LST.

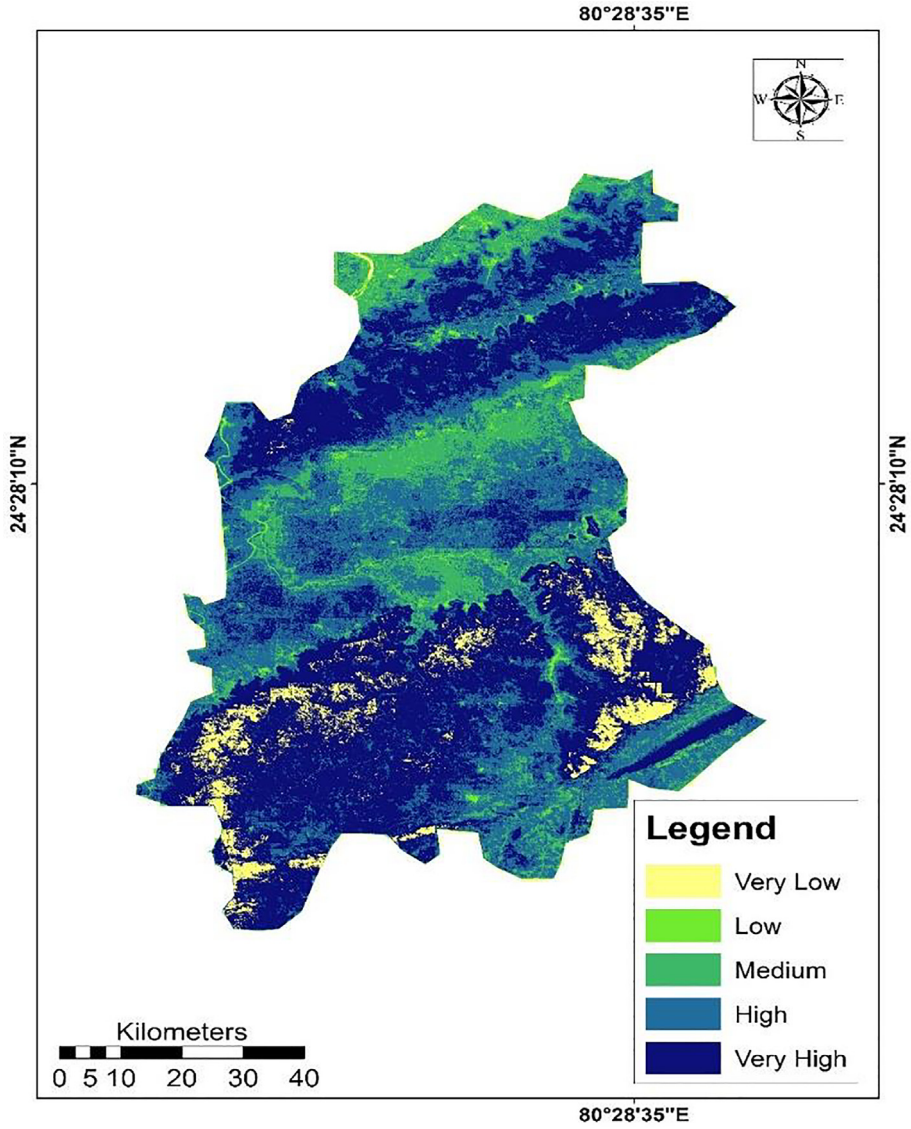

Fig. 6. Groundwater Availability of area.

groundwater potential areas by mixing LULC datasets, LST data, and hydrological system. The outcomes acquired from Arc GIS 10.5 deliver valuable visions into parts with variation water levels of groundwater obtainability, helping in expressing real groundwater management policies. The results found in this paper and the application of GEE, RS, and Arc GIS 10.5 for groundwater estimation suggestion valuable inputs for policymakers and stakeholders in applying effective processes for watershed conservation and LULC planning in the area.

12.1. Discussion

Urbanization is a composite and lively procedure (Li et al., 2022). Urbanization alters forest and vegetation cover into residences, production industries, roads, and current conveniences (Patra et al., 2018). LULC variations ensue at urban borders due to quick built-up development associated with population compression and commercial expansion (Haldar et al., 2023). Comparisons of previous studies are totally different compared to current results of the LULC change, NDVI and LST maps created and related to groundwater availability. Very fast urbanization raises resistant layers such as buildings, water bodies, vegetation, roads and industries. It may vary in LULC classes, and main to large LSTs also impact the climate (Njoku & Tenenbaum, 2022; Xie et al., 2023). LST replicates how much the Earth's external is intense by dissimilar classes of LULC (Kayet et al., 2016). The alteration of LULC is the main reason for LST differences. Dissimilar LULC kinds have separate energy reproduction and absorption abilities (Ara et al., 2021). Higher LST and urban heat islands (UHI) are more damaging consequences of urbanization (Choudhury et al., 2021).

Deng et al. (2018) found clear differences in LST crosswise forest, bodies, roads, and urban land. These differences propose that LULC kinds disturb native temperatures otherwise. Kafy et al. (2020) examined the influence of LULC variations on LST and the connection among spectral indices such as NDVI, normalized difference built-up index (NDBI), and LST. LULC classes day by day changes rapidly due to climate change and increases urban expansion and air pollution with impact on the natural resources Saha et al. (2021) surveyed the suggestion among LULC and LST in three important capitals of eastern India and decided that built-up land has increases LST, while internal city regions have maximum UHI value. Chatterjee and Majumdar (2022) observed the influence of fast urban expansion on the UHI in India, found that LST is higher in the urban core and vegetation reductions to the urban center.

Our studies developed the algorithms for preparation of spatial maps of LST, NDVI and LULC maps using GEE, which is parameters is related and impact on the groundwater availability. This is important results and novel approach adopted in the study as compared with previous studies and mentioned in the discussion section.

13. Conclusion

In this paper remote sensing, GIS, and GEE are used to evaluate the impact of urbanization on groundwater in Panna district, Madhya Pradesh. Accurate land use classification using the random forest technique showed that built-up areas expanded over the years, leading to higher LST and affecting the groundwater in the region. The reduction in surface water bodies and the undesirable correlation between LST and NDVI further emphasized the ecological consequences of urban growth. Moreover, the study highlighted the critical importance of water resources for sustaining life in the region. Due to a 31 % rain deficiency and irregular rainfall patterns, groundwater recharge needed to increase, exacerbating water scarcity issues. Consequently, people resorted to digging bore wells, further depleting the already strained groundwater levels. The findings underscore the intricate relationship between hydrological features, vegetation cover, and climate factors. With declining vegetation cover due to urbanization and rising LST, the availability of water resources is likely to decrease. Implementing water regeneration structures and measures to increase vegetation cover is crucial to mitigate these adverse effects. This research highlights the vulnerability of the Bundelkhand region, especially the Panna district, to the consequences of climate change. It emphasizes the urgent need for government intervention to address water-related challenges and promote sustainable land use practices to safeguard the area's ecosystems and ensure the well-being of its inhabitants.

14. Future research/way

The current research investigation requires an extra study into the influences among built-up, land use and cover variations, and groundwater assets. Now a days climate change variables Upcoming efforts should improve land use classes, include high-resolution datasets, and spread temporal investigation to cover continuing developments well. Weather models also suggest visions of how built-up growth affects the water resources below atmospheric variation situations. Future research focuses on predicting the LST, LULC and groundwater zone mapping for future forecasting of climate models. Future research more climate datasets and observation of water level information could use to for what impact of climate variables and LULC change on the groundwater resources and surface water. Currently, more advanced the technologies such as ML, remote sensing and GIS are used for high-resolution datasets of the LST impact on the groundwater resources and water level trend. Future work should discover the socio-economic drivers of expansion and examine nature-based results, such as cumulative vegetation protection, to moderate increasing LST and improve groundwater refresh. This investigation is vital to keep water resources and environmental conditions in vulnerable areas in the Bundelkhand area.

15. Limitations of study

The study investigation's limitations include the support of GEE and remote sensing data, which, while useful, may not grab whole local ground-level changes and dynamics precisely. The temporal resolution of satellite images may also skip short-term differences in LULC classes. Also, although robust, the RF model LULC classification may have restrictions in differentiating among the same pixels to classify different Landover classes. The analysis focuses on the Panna district, and outcomes may not presently be employed in other regions with various climatic or geological conditions. The lack of long-term field data further limits the validation of results and the understanding of seasonal changes.

CRediT authorship contribution statement

Kanak N. Moharir: Conceptualization, Formal analysis, Validation, Investigation, Methodology, Visualization, Writing – original draft, Writing – review & editing. **Chaitanya Baliram Pande:** Investigation, Methodology, Visualization, Writing – original draft, Writing – review & editing. **Vinay Kumar Gautam:** Visualization, Writing – original draft, Writing – review & editing. **Sonam Sandeep Dash:** Formal analysis, Writing – original draft. **Arun Pratap Mishra:** Data curation, Formal analysis, Writing – original draft. **Krishna Kumar Yadav:** Formal analysis,

Validation, Writing – review & editing. **Malay Pramanik:** Investigation, Validation, Writing – original draft, review & editing. **Mohamed Elsahabi:** Formal analysis, Validation, Writing – review & editing.

Declaration of competing interest

The authors declare that they have no known competing financial interests or personal relationships that could have appeared to influence the work reported in this paper.

Acknowledgement

The authors extend their appreciation to the Researchers Supporting Project number (RSPD2024R812), King Saud University, Riyadh, Saudi Arabia, for funding this work.

References

Abdullah, A., Masrur, A., Adnan, M., Baky, M., Hassan, Q., Dewan, A., 2019. Spatio-temporal patterns of land use/land cover change in the heterogeneous coastal region of Bangladesh between 1990 and 2017. Remote Sens. (Basel) 11 (7), 790.

Abera, T.A., Heiskanen, J., Pellikka, P., Rautiainen, M., Maeda, E.E., 2019. Clarifying the role of radiative mechanisms in the spatio-temporal changes of land surface temperature across the Horn of Africa. Remote Sens. Environ. 221, 210–224.

Abou Samra, R.M., 2022. Dynamics of human-induced lakes and their impact on land surface temperature in Toshka Depression, Western Desert, Egypt. Environ. Sci. Pollut. Res. 29, 20892–20905.

Abou Samra, R.M., 2023. Investigating and mapping day-night urban heat island and its driving factors using Sentinel/MODIS data and Google Earth Engine. Case study: Greater Cairo, Egypt. Urban Clim. 52, 101729.

Abou Samra, R.M., El-Barbary, S.M., 2018. The use of remote sensing indices for detecting environmental changes: a case study of North Sinai. Egypt Spatial Information Research 26, 679–689. https://doi.org/10.1007/s41324-018-0211-1.

Akhtar, F., Awan, U.K., Tischbein, B., Liaqat, U.W., 2020. A phenology based geo-informatics approach to map land use and land cover (2003–2013) by spatial segregation of large heterogenic river basins. Appl. Geogr. 88, 48–61.

Ali, A., Khalid, A., Butt, M.A., Mehmood, R., Mahmood, S.A., Sami, J., Ali, F., 2018. Towards a remote sensing and GIS-based technique study population and urban growth: a case study of Multan. AdvRemote Sens 7 (3), 245–258.

Ara et al., 2021. Impact of tourism on LULC and LST in a coastal island of Bangladesh: A geospatial approach on St. Martin's Island of Bay of Bengal, J. Indian Soc. Remote Sens. 49(10), 2329–2345.

Athick, A.M.A., Shankar, K., Naqvi, H.R., 2019. Dataon time series analysis of land surface temperature variation in response to vegetation indices in twelve Wereda of Ethiopia using mono window, split window algorithm and spectral radiance model. Data Brief 27, 104773.

Babalola, O.S., Akinsanola, A.A., 2020. Change detection in land surface temperature and land use land cover over Lagos Metropolis. Nigeria J Remote Sens GIS 5 (3), 10–4172.

Bansod, R.D., Dandekar, U.M., 2018. Evaluation of Morna river catchment with RS and GIS techniques. J. Pharmacogn. Phytother. 7 (1), 1945–1948.

Begum, M., Bala, S., Islam, A., Islam, G., Roy, D., 2021. An analysis of spatio-temporal trends of land surface temperature in the Dhaka metropolitan area by applying landsat images. J. Geogr. Inf. Syst. 13, 538–560.

Cai, M., Ren, C., Xu, Y., Lau, K.K.L., Wang, R., 2018. Investigating the relationship between local climate zone and land surface temperature using an improved WUDAPT methodology–A case study of Yangtze River Delta, China. Urban Clim. 24, 485–502.

CGWB, 2013. District groundwater information booklet. Ministry of Water Resources, Govt. of India.

Chatterjee, U., Majumdar, S., 2022. Impact of land use change and rapid Urbanization on urban heat island in Kolkata city: A remote sensing based perspective. J. Urban Manag. 11 (1), 59–71.

Choudhury et al., 2021. Investigating thermal behavior pattern (TBP) of local climatic zones (LCZs): A study on industrial cities of Asansol-Durgapur development area (ADDA), eastern India. Urban Clim 35, 10072. https://doi.org/10.1016/j.uclim.2020.100727.

Deng et al., 2018. Relationship among land surface temperature and LUCC, NDVI in typical karst area. Sci Rep. 8 (1), 641. https://doi.org/10.1038/s41598-017-19088-x.

Kamyar Fuladlu. 2022. Thermal Response to Land-Use Land-Cover Patterns: An Experimental Study in Famagusta, Cyprus. Clean Soil Air Water 31 July 2022.

Gautam, V.K., Trivedi, A., 2023. Optimal water resources allocation and crop planning for Mandla district of Madhya Pradesh. Indian J. Soil Conser. 51, 1–8.

Gautam, V.K., Awasthi, M.K., Trivedi, A., 2020. Optimum allocation of water and land resource for maximizing farm income of Jabalpur District, Madhya Pradesh. Inter. J. Environ. Climate Change 10 (12), 224–232.

Gautam, V.K., Kothari, M., Singh, P.K., Bhakar, S.R., Yadav, K.K., 2021a. Determination of geomorphological characteristics of Jakham River Basin using GIS technique. Indian J. Ecology 48 (6), 1627–1634.

Gautam, V.K., Kothari, M., Singh, P.K., Bhakar, S.R., Yadav, K.K., Singh, M., 2021b. Analysis of groundwater level for detection of trend in Jakham river basin of southern Rajasthan using geospatial technique. J. Ground. Sci. Eng. 10 (1), 1–9.

Gautam, V.K., Kothari, M., Singh, P.K., Bhakar, S.R., Yadav, K.K., 2022. Decadal groundwater level changes in Pratapgarh district of Southern Rajasthan. India. Ecology Environment & Conservation 28 (1), 283–289.

Gautam, V.K., Pande, C.B., Moharir, K.N., Varade, A.M., Rane, N.L., Egbueri, J.C., Alshehri, F., 2023a. Prediction of sodium hazard of irrigation purpose using artificial neural network modelling. Sustainability 15 (9), 7593.

Gautam, V.K., Pande, C.B., Kothari, M., Singh, P.K., Agrawal, A., 2023b. Exploration of groundwater potential zones mapping for hard rock region in the Jakham river basin using geospatial techniques and aquifer parameters. Adv. Space Res. 71 (6), 2892–2908.

Guo, B., Zhou, Y., Wang, S.X., Tao, H.P., 2014. The relationship between normalized difference vegetation index (NDVI) and climate factors in the semiarid region: A case study in Yalu Tsangpo River basin of Qinghai-Tibet Plateau. J. Mt. Sci. 11 (4), 926–940. https://doi.org/10.1007/s11629-013-2902-3.

Haldar, et al., 2023. Dynamicity of land use/land cover (LULC): An analysis from peri-urban and rural neighbourhoods of Durgapur Municipal Corporation (DMC) in India Regional Sustainability 4(2), 150-172.

He, L., Valocchi, A.J., Duarte, C.A., 2024. An adaptive global-local generalized FEM for multiscale advection-diffusion problems. Comput. Methods Appl. Mech. Eng. 418, 116548. https://doi.org/10.1016/j.cma.2023.116548.

Hussain, S., Karuppannan, S., 2023. Land use/land cover changes and their impact on land surface temperature using remote sensing technique in district Khanewal, Punjab Pakistan. Geology, Ecology, and Landscapes 7 (1), 46–58.

Hussain, S., Mubeen, M., Ahmad, A., Akram, W., Hammad, H.M., Ali, M., et al., 2020a. Using GIS tools to detect the land use/land cover changes during forty years in Lodhran District of Pakistan. Environ. Sci. Pollut. Res. 27, 39676–39692.

Hussain, S., Mubeen, M., Akram, W., Ahmad, A., Habib-ur-Rahman, M., Ghaffar, A., et al., 2020b. Study of land cover/land use changes

using RS and GIS: a case study of Multan district, Pakistan. Environ. Monit. Assess. 192, 1–15.
Hussain, S., Lu, L., Mubeen, M., Nasim, W., Karuppannan, S., Fahad, S., et al., 2022a. Spatiotemporal variation in land use land cover in the response to local climate change using multispectral remote sensing data. Land 11 (5), 595.
Hussain, S., Mubeen, M., Ahmad, A., Majeed, H., Qaisrani, S.A., Hammad, H.M., et al., 2022b. Assessment of land use/land cover changes and its effect on land surface temperature using remote sensing techniques in Southern Punjab, Pakistan. Environ. Sci. Pollution Res., 1–17
Hussain, S., Raza, A., Abdo, H.G., Mubeen, M., Tariq, A., Nasim, W., et al., 2023. Relation of land surface temperature with different vegetation indices using multi-temporal remote sensing data in Sahiwal region, Pakistan. Geosci. Lett. 10 (1), 33.
Kabeto, J., Adeba, D., Regasa, M.S., Leta, M.K., 2022. Groundwater potential assessment using GIS and remote sensing techniques: case study of West Arsi zone. Ethiopia, Water 14, 1838.
Kafy et al., 2020. Modelling future land use land cover changes and their impacts on land surface temperatures in Rajshahi, Bangladesh Remote Sens. Appl.: Soc. Environ. 18, 100314. https://doi.org/10.1016/j.rsase.2020.100314.
Kayet et al., 2016. Spatial impact of land use/land cover change on surface temperature distribution in Saranda Forest, Jharkhand Model. Earth Syst. Environ. 2. https://doi.org/10.1007/s40808-016-0159-x.
Khan, R., Gilani, H., Iqbal, N., Shahid, I., 2020a. Satellite-based (2000–2015) drought hazard assessment with indices, mapping, and monitoring of Potohar plateau, Punjab, Pakistan. Environ. Earth Sci. 79 (1), 23.
Khan, M.J., Zeeshan, M.M., Ali, S.S., 2020b. Gis-based change detection of coastal features along Karachi coast Pakistan. Pak. J. Sci. 72 (2), 124.
Kharazmi, R., Tavili, A., Rahdari, M.R., Chaban, L., Panidi, E., Rodrigo-Comino, J., 2018. Monitoring and assessment of seasonal land cover changes using remote sensing: A 30-year (1987–2016) case study of Hamoun Wetland, Iran. Environ. Monitor. Assessment 190 (6), 356.
Kimuku, C.W., and Ngigi, M.M. 2017. Study of urban heat island trends to aid in urban planning in Nakuru County-Kenya.
Li et al., 2022. Spatio-temporal evolution and driving mechanism of Urbanization in small cities: Case study from Guangxi Land 11(3), 415, 10.3390/land11030415.
Li, Z., He, M., Li, B., Wen, X., Zhou, J., Cheng, Y., et al., 2024. Multi-isotopic composition (Li and B isotopes) and hydrochemistry characterization of the Lakko Co Li-rich salt lake in Tibet, China: Origin and hydrological processes. J. Hydrol. 630, 130714. https://doi.org/10.1016/j.jhydrol.2024.130714.
Li, J., Pang, Z., Liu, Y., Hu, S., Jiang, W., Tian, L., et al., 2023. Changes in groundwater dynamics and geochemical evolution induced by drainage reorganization: Evidence from 81Kr and 36Cl dating of geothermal water in the Weihe Basin of China. Earth Planet. Sci. Lett. 623, 118425. https://doi.org/10.1016/j.epsl.2023.118425.
Liu, C., Shan, Y., He, L., Li, F., Liu, X., et al., 2024. Plant morphology impacts bedload sediment transport. Geophys. Res. Lett. 51 (12), e2024GL108800. https://doi.org/10.1029/2024GL108800.
Moharir, K.N., Pande, C.B., Gautam, V.K., Singh, S.K., Rane, N.L., 2023. Integration of hydrogeological data, GIS and AHP techniques applied to delineate groundwater potential zones in sandstone, limestone and shales rocks of the Damoh district, (MP) central India. Environ. Res. 228, 115832.
Mukherjee, F., Singh, D., 2020. Assessing land use–land cover change and its impact on land surface temperature using LANDSAT data: A comparison of two urban areas in India. Earth System Environment 4 (2), 385–407.
Njoku and Tenenbaum, 2022. Quantitative assessment of the relationship between land use/land cover (LULC), topographic elevation and land surface temperature (LST) in Ilorin, Nigeria, Remote Sens. Appl.: Soc. Environ., 27, 100780, 10.1016/j.rsase.2022.100780.
Pal, S., Ziaul, S.K., 2017. Detection of land use and land cover change and land surface temperature in English Bazar urban centre. Egyptian Remote Sens Space Sci 20 (1), 125–145.
Pande, 2022. Land use/land cover and change detection mapping in Rahuri watershed area (MS), India using the google earth engine and machine learning approach Geocarto Int. 10.1080/10106049.2022.2086622.
Patra et al., 2018. Impacts of urbanization on land use/cover changes and its probable implications on local climate and groundwater level. J. Urban Manag. 7 (2), 70–84.
Peng, J., Xie, P., Liu, Y., Ma, J., 2019. Urban thermal environment dynamics and associated landscape pattern factors: A case study in the Beijing metropolitan region. Remote Sens. Environ. 173, 145–155.
Rambe, B.A. 2020. Karakteristik Distribusi Spasial dan Analisis Pakan Satwa Mangsa Harimau Sumatera (Panthera Tigris Sumatrae) di Seksi Pengelolaan Taman Nasional (Sptn) Vi Besitang, Taman Nasional Gunung Leuser (TNGL).
Romaguera, M., Vaughan, R.G., Ettema, J., Izquierdo- Verdiguier, E., Hecker, C.A., Van der Meer, F.D., 2018. Detecting geothermal anomalies and evaluating LST geothermal component by combining thermal remote sensing time series and land surface model data. Remote Sens. Environ. 204, 534–552.
Roy, B., Bari, E., Nipa, N.J., Ani, S.A., 2021. Comparison of temporal changes in urban settlements and land surface temperature in Rangpur and Gazipur Sadar, Bangladesh after the establishment of city corporation. Remote Sens. Appl.: Soc. Environ. 23, 100587.
Sadiq Khan, M., Ullah, S., Sun, T., Rehman, A.U., Chen, L., 2020. Land-use/land-cover changes and its contribution to urban heat island: A case study of Islamabad, Pakistan. Sustainability 12 (9), 3861.
Safder, Q., 2019. Assessment of urbanization and urban sprawl analysis through remote sensing and GIS: A case study of Faisalabad, Punjab, Pakistan. Inter. J. Acad. Res. Busin. Social Sci. 9 (4).
Saha, S. et al. 2021. Analyzing spatial relationship between land use/land cover (LULC) and land surface temperature (LST) of three urban agglomerations (UAs) of Eastern India, Remote Sens. Appl.: Soc. Environ., 22, 100507, 10.1016/j.rsase.2021.10050.
Sajan, B., Kanga, S., Singh, S.K., Mishra, V.N., Durin, B., 2023. Spatial variations of LST and NDVI in Muzaffarpur district, Bihar using Google earth engine (GEE) during 1990–2020. Journal of Agrometeorology 25 (2), 262–267.
Salahi, B., Behrouzi, M., 2023. Modeling of land surface temperature (LST) in Ardabil plain using NDVI index and Bayesian neural network approach. Model. Earth Syst. Environ., 1–10
Song, X., Hansen, M.C., Stehman, S.V., Potapov, P.V., Tyunkvina, A., Vermote, E.F., Townshend, J.R., 2018. Global land change from 1982 to 2016. Nature 560 (7720), 639–643.
Tafesse, B., Suryabhagavan, K.V., 2019. Systematic modeling of impacts of land-use and land-cover changes on land surface temperature in Adama Zuria District. Ethiopia. Model Earth Syst Environ 5 (3), 805–817.
Trivedi, A., Gautam, V.K., 2022. Decadal analysis of water level fluctuation using GIS in Jabalpur district of Madhya Pradesh. J. Soil Water Conserv. 21 (3), 250–259.
Vohra, R., Tiwari, K.C., 2023. Analysis of land use and land cover changes and their impact on temperature using landsat satellite imageries. Environ. Dev. Sustain. 25, 8623–8650.
Waleed, M., Mubeen, M., Ahmad, A., Habib-ur-Rahman, M., Amin, A., Farid, H.U., et al., 2022. Evaluating the efficiency of coarser to finer resolution multispectral satellites in mapping paddy rice fields using GEE implementation. Sci. Rep. 12 (1), 13210.
Wang, L., Wang, Z., Yu, J., Zhang, Y., Dang, S., 2018. Hydrological process simulation of inland river watershed: a case study of the heihe river basin with multiple hydrological models. Water 10.
Xie, D., Huang, H., Feng, L., Sharma, R.P., Chen, Q., Liu, Q., et al., 2023. Aboveground biomass prediction of arid shrub-dominated community based on airborne LiDAR through parametric and nonparametric methods. Remote Sens. (Basel) 15 (13), 3344. https://doi.org/10.3390/rs15133344.

Yamamoto, Y., Ishikawa, H., 2020. Influence of urban spatial configuration and sea breeze on land surface temperature on summer clear sky days. Urban Clim. 31, 100578.

Yi, J., Li, H., Zhao, Y., Shao, M., Zhang, H., et al., 2022. Assessing soil water balance to optimize irrigation schedules of flood-irrigated maize fields with different cultivation histories in the arid region. Agric Water Manag 265, 107543. https://doi.org/10.1016/j.agwat.2022.107543.

Yin, L., Wang, L., Keim, B.D., Konsoer, K., Zheng, W., 2022. Wavelet Analysis of Dam Injection and Discharge in Three Gorges Dam and Reservoir with Precipitation and River Discharge. Water 14 (4), 567. https://doi.org/10.3390/w14040567.

Yin, L., Wang, L., Li, T., Lu, S., Yin, Z., Liu, X., et al., 2023a. U-Net-STN: A Novel End-to-End Lake Boundary Prediction Model. Land 12 (8), 1602. https://doi.org/10.3390/land12081602.

Yin, L., Wang, L., Keim, B.D., Konsoer, K., Yin, Z., Liu, M., et al., 2023b. Spatial and wavelet analysis of precipitation and river discharge during operation of the Three Gorges Dam. China. Ecological Indicators 154, 110837. https://doi.org/10.1016/j.ecolind.2023. 110837.

Zhang, K., Li, Y., Yu, Z., Yang, T., Xu, J., Chao, L., et al., 2022. Xin'anjiang nested experimental watershed (XAJ-NEW) for understanding multiscale water cycle: scientific objectives and experimental design. Engineering 18 (11), 207–217. https://doi.org/10.1016/j.eng.2021.08.026.

Zhao, Y., Wang, H., Song, B., Xue, P., Zhang, W., Peth, S., et al., 2023. Characterizing uncertainty in process-based hydraulic modeling, exemplified in a semiarid Inner Mongolia steppe. Geoderma 440, 116713. https://doi.org/10.1016/j.geoderma.2023.116713.

Zhao, Y., Li, J., Wang, Y., Zhang, W., Wen, D., 2024a. Warming climate-induced changes in cloud vertical distribution possibly exacerbate intra-atmospheric heating over the tibetan plateau. Geophysical Research Letters 51 (3), e2023GL107713. https://doi.org/10.1029/2023GL107713.

Zhao, Y., Lu, M., Chen, D., Zhang, L., 2024b. Understanding the weakening patterns of inner Tibetan Plateau vortices. Environ. Res. Lett. 19 (6), 064076. https://doi.org/10.1088/1748-9326/ad5193.

Zhou, G., Xu, J., Hu, H., Liu, Z., Zhang, H., Xu, C., et al., 2023a. Off-axis four-reflection optical structure for lightweight single-band bathymetric LiDAR. IEEE Trans. Geosci. Remote Sens. 61. https://doi.org/10.1109/TGRS.2023.3298531.

Zhou, G., Zhang, H., Xu, C., Zhou, X., Liu, Z., Zhao, D., et al., 2023b. A Real-Time Data Acquisition System for Single-Band Bathymetric LiDAR. IEEE Trans. Geosci. Remote Sens. 61. https://doi.org/10.1109/TGRS.2023.3282624.

Zhou, G., Lin, G., Liu, Z., Zhou, X., Li, W., Li, X., et al., 2023c. An optical system for suppression of laser echo energy from the water surface on single-band bathymetric LiDAR. Opt. Lasers Eng. 163, 107468. https://doi.org/10.1016/j.optlaseng.2022.107468.